Biophysical Journal
Article

Biophysical Society

Dynamics of Cell Membrane Permeabilization by Saponins Using Terahertz Attenuated Total Reflection

Xiujun Zheng[1] and Guilhem Gallot[1,*]
[1]LOB, École Polytechnique, CNRS, INSERM, Institut Polytechnique de Paris, Palaiseau, France

ABSTRACT Understanding the relevant parameters of the formation of pores during permeabilization is very challenging for medical applications. Several components are involved: the arrival of the permeabilizing molecules to the membrane, the efficiency of formation of the pores and their specific dynamics, and the flux of molecules through the plasma membrane. Using attenuated total reflection in the terahertz domain, we studied the dynamics of Madine-Darby canine kidney cells after permeabilization by saponin molecules. We developed an analytical model taking into account saponin molecule diffusion, cell geometry, cytosol molecule diffusion, and pore dynamics. We also studied the effect of possible pore overlapping on the cell membrane, introducing a dimensionless quantity that is the ratio between overlapping and diffusive effects. Pores are found to be static within 1 h after their creation, hinting that the diffusion of the saponin molecules to the membrane is the limiting factor in our experiments.

SIGNIFICANCE This study is of particular interest for the controlled delivery of specific molecules through the cell membrane, such as in gene therapy, treatment against cancer, and biotechnology. It provides original experiments and modeling of detergent permeabilization of cell membrane. In particular, measurements in the terahertz domain demonstrate the probing of cytosol leakage by optical techniques without specific staining or labeling.

INTRODUCTION

Biological membranes play a major role in the cellular protection, as well as in the transport and control of nutrients. The plasma membrane constitutes a fundamental barrier for the entry of hydrophilic molecules into the cell interior. The selective and controlled permeabilization of this barrier is a condition for many biotechnological and medical applications (1–3): cell-based gene therapy; biomanufacture of proteins, vectors, and antibodies; regenerative medicine of engineered tissues; disease modeling; treatment against cancer; drug screening; and diagnostics and analysis. Possible delivered substances are gene-editing molecules, DNA, RNA, proteins, metabolites, peptides, membrane-impermeable drugs, antibodies, engineered probes, etc. A cell becomes permeable after the weakening of the plasma membrane to the point of creating a pore. The plasma membrane can be disrupted by physical means such as electroporation, mechanical force, optoporation, and thermal effect, as well as by biochemical techniques, the most eminent of which are pore-forming toxins and detergents (4). Many active mechanisms exist for repairing the cell membrane after pore formation, and they seem to depend relatively little on the origin of the damage whether the source is electrical, mechanical, or chemical (5). These mechanisms mostly depend on the pore size, temperature, and cell medium. After plasma membrane disruption, the defect evolution is the result of two opposing forces. Surface pressure tends to increase the defect, whereas line tension favors a shrinking of the membrane and a pore size reduction (6,7). In electroporation, pores are typically found to exponentially decrease on a timescale of minutes or tens of minutes (8,9). Plasma membrane can exhibit growth or decay of the pores (10), and exponential defect growth is also found in polymer membranes (11). Studying the relevant parameters for pore formation and dynamics is therefore very important for developing pore models and for medical and industrial applications.

Detergents act by solubilizing the components of the membranes. Amphiphilic plant glycoside saponins are the most popular detergents for reversible cell permeabilization.

Submitted January 24, 2020, and accepted for publication May 4, 2020.
*Correspondence: guilhem.gallot@polytechnique.edu
Editor: John Conboy.
https://doi.org/10.1016/j.bpj.2020.05.040

Although the exact mechanisms are still being studied, it is known that saponins interact with membrane cholesterol, making them more specific to cholesterol-rich plasma membranes (1). Detergents can penetrate the lipid bilayer membrane and induce constrains that distort the membrane, thus leading to a weakening of the bilayer and the formation of pores (12). To study cell permeabilization, the terahertz domain exhibits many advantages. It is directly sensitive to ions and proteins in solution, contrary to the visible domain; absorption is far less important than in the infrared; and it offers better sensitivity than the hyperfrequency domain (13). Recent works demonstrated the possibility of spectroscopically investigating complex systems such as cells and even tissues or small organs (13–17). Using a terahertz attenuated total reflection (THz-ATR) device designed for biological samples, we demonstrated the possibility of using THz sensitivity to follow permeabilization dynamics of live monolayer MDCK cells in real time, without any marker or sample preparation (18). The origin of the terahertz contrast was also investigated and was found to be related to the modification of the dielectric constant of liquid water in the presence of solutes such as ions, peptides, and proteins (19). Here, the permeabilization of the plasma membrane by saponins was followed by sensing in the terahertz domain. An analytical model describes the relevant physical parameters: the diffusion of saponin molecules, their binding efficiency to the plasma membrane, the specific pore dynamics, and the effusion of the cytosol molecules through the pores.

MATERIALS AND METHODS

Cell growth

Madine-Darby canine kidney (MDCK) cells are an immortal cell line derived from dog kidney. They are widely used as a model cell line for studies on epithelial polarization and transport, mechanisms of infection, regulation of tight junctions, etc. (20). These cells form a typical cuboidal single layer epithelium when grown to confluence, at which they display a height of 10–12 μm (21). MDCK cells were maintained in Dulbecco's modified Eagle's medium (61965026; Thermo Fisher Scientific, Waltham, MA) supplemented with 10% fetal bovine serum (10500064; Thermo Fisher Scientific), 1% penicillin-streptomycin (15140122; Thermo Fisher Scientific) at 37°C and 5% CO_2. Cells were isolated with trypsin-EDTA (R001100; Thermo Fisher Scientific), passed on silicon plate (for experimental purposes) in culture medium, and grown until confluence. Half of the layer was kept on the plate, whereas the other half was scratched free as a reference. Before each experiment, the plate was washed with PBS (phosphate-buffered saline, 20012019; Thermo Fisher Scientific) solution and allowed to reach room temperature (21°C) in 3 mL of PBS. Because the plate diameter is 36 mm, the cells were covered by a 3 mm height of solution. The cells density was ~20,000 per cm^2, counted with a Malassez hemocytometer (Thermo Fisher Scientific), before culturing during 72 $\pm$ 4 h.

Saponin detergent

Saponins are glycosides mainly produced by plants that form soap-like foams in solution. Saponins consist of a sugar moiety linked to a hydrophobic aglycone (22). A great variety of saponins are found, depending on the nature of the aglycone, side chains, and relative positions (23). Saponins at high concentrations are more commonly used in immunocytochemistry to permeabilize membranes of different kind of fixed cells but have also been reported to permeabilize live-cell plasma membrane at low concentrations and in a reversible way (24). They are nonionic detergents that create nonspecific pores in cell membrane, most probably by binding with the cholesterol within the lipid components of the cell membrane (22). They can mostly trigger protein and ion transfers through the membrane. Saponins used (47036; Sigma-Aldrich, St. Louis, MO) were a mixture of sapogenin molecules at a mass fraction f = 8–25%, so the exact quantity of saponin is unknown. All the experiments were done with the same saponin sample to preserve the direct comparison between the experiments. The saponin number concentration C_0 is related to the mass concentration c_0 of the commercial saponin as

$$C_0 = \frac{f \mathcal{N}_A \, c_0}{M}, \tag{1}$$

where $\mathcal{N}_A$ is Avogadro's constant and M the molar mass.

THz-ATR measurements

THz-ATR makes use of the evanescent wave at the back of a prism under total internal reflection, which is coupled to the sample under study (Fig. 1). When light is reflected at the interface of two optical media with $n_1 > n_2$, total reflection occurs for $n_1 \sin\theta > n_2$, and an evanescent field exists in the less optically dense medium n_2 (Fig. 1 *B*). When a sample is put on top of the prism, the evanescent wave extends into the sample. The measurement of the reflected beam is then directly correlated with the complex

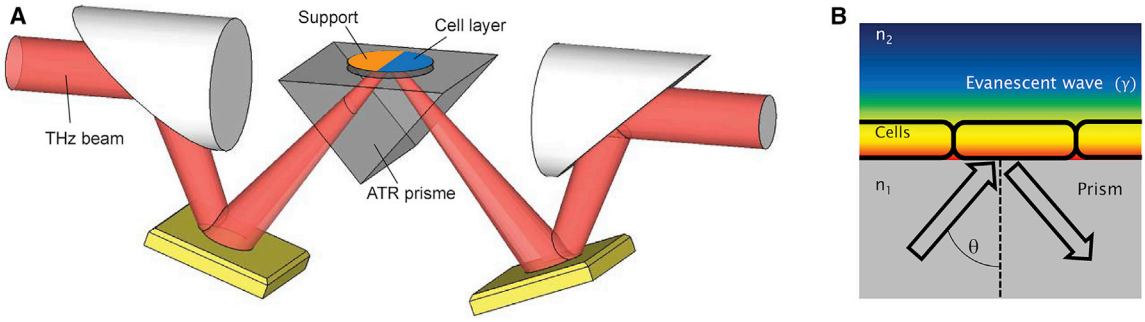

FIGURE 1 THz-ATR device inserted in the THz-TDS setup. (*A*) The sample is located on top of a silicon support put in close contact with the top of the silicon prism. The support can be translated. Polarization is in the incident plane (p-polarization). (*B*) Close view of the ATR prism is shown. The cell layer lies in the evanescent field zone (in *color gradient*). To see this figure in color, go online.

refractive index of the medium topping the prism. The penetration depth of the evanescent field depends on the beam wavelength and on the refractive index of the prism and of the topping medium. The penetration depth of the evanescent field depends on the beam wavelength and on the dielectric constants of the prism and of the topping medium. More precisely, we consider a thin layer of cells and the surrounding solution in this inhomogeneous evanescent wave. Providing that the thickness of the cell layer matches the penetration depth of the evanescent wave, the reflected terahertz wave is modified by the terahertz dielectric properties of the cell layer in contact with the top of the prism. The stronger coupling is obtained for a penetration depth of the same value as the cell layer thickness. The resulting reflected terahertz signal is then correlated with the cytosol content. The extracellular solution above the cell layer only weakly affects the terahertz signal because its volume is much larger than the intracellular one. Therefore, cytosol leakage from the cell to the surrounding solution can easily be detected by the change of the cell content (18,19).

The terahertz signal was generated by a terahertz time-domain spectroscopy (THz-TDS) setup (25,26) composed of a galium arsenide (GaAs) photoconductive transmitter lit by a femtosecond laser that generated subcycle THz pulses, with frequencies centered around 0.5 THz and extending from 0.2 to 1 THz. The THz pulse was detected by a low-temperature-grown GaAs photoconductive detector that was sensitive to the electric field of the wave. A delay line between the emitter and detector terahertz chips allowed the direct sampling out of the amplitude $A(t)$ of the terahertz electric field in the time domain. An ATR prism (see Fig. 1 *a*) was added to the THz-TDS setup and generated the evanescent wave at its back and sensed the cells under study (27). The THz-ATR prism was a very transparent high-resistivity silicon isosceles prism ($n \approx 3.42$) with a base angle of 42°. Because of the frequency range, the evanescent field generated at the surface of the prism and interacting with the sample is the weighted average of the fields for all the frequencies. The result is an effective evanescent field whose penetration depth is ~15 μm in our experimental conditions (27). The penetration depth remains always constant during the experiments because the frequency range is constant. The impinging beam was polarized in the plane of incidence (p-polarization). Its reflection coefficient depends on both absorption and refractive index of the sample topping the prism. MDCK cells were grown on a high-resistivity 3-mm-thick silicon window put in close contact with the prism. Flatness for both prism and window surfaces was better than 1 μm over the whole surface to provide optical continuity between the prism and the windows, without index matching material. The window was translated during data acquisition by a motorized translation stage so that acquisitions were done either in the cell or reference PBS areas. Peak amplitude (PA) of $A(t)$ was chosen as it demonstrated the strongest sensitivity between cells and PBS zones (18). We define the relative Δ_{rel} and normalized Δ experimental contrasts

$$\Delta(t) = \frac{\Delta_{\mathrm{rel}}(t)}{\Delta_{\mathrm{rel}}(t\ =\ 0)} \quad \text{with} \quad \Delta_{\mathrm{rel}}(t)\ =\ \frac{\mathrm{PA_{cell}}(t) - \mathrm{PA_{ref}}(t)}{\mathrm{PA_{ref}}(t)}, \tag{2}$$

where $\mathrm{PA_{ref}}$ and $\mathrm{PA_{cell}}$ are the PA in PBS reference and cell zones, respectively, obtained by moving the sample windows with the motorized translation stage. Perturbation was applied to the cells at time $t = 0$. For each position, the PA-value was obtained in 0.25 s. The cell layers typically displayed a 7–8% PA relative contrast Δ_{rel} compared with PBS alone.

Modeling

The system is considered to be a uniform cell layer (see Fig. 2). The basal plasma membrane is in contact with the silicon substrate, whereas the apical membrane is in direct contact with saponin molecules in solution in PBS. The saponin molecules can move freely in the liquid by diffusion or sedimentation. Once a molecule encounters the apical membrane, it creates a pore with a given probability, increasing the total number of pores with time. Then, effusion of molecules through the pores takes place and changes the concentration of molecules in the cytosol. The saponin concentration of the solution is not considered to be modified because the PBS/saponin solution volume is by far much larger than that of the cytosol. The concentration of saponins is also assumed to be lower than the critical micelle concentration at which saponins start to aggregate. Once the pores are created by the saponin molecules, we will consider two possible individual behaviors: an exponential growth or shrinkage of pores.

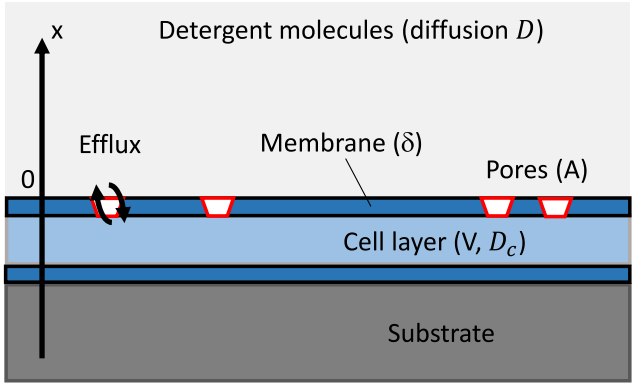

FIGURE 2 Model of the pore formation mechanism on the cell membrane. The cell layer is put on top of the prism substrate. To see this figure in color, go online.

In the following, the model is reduced by symmetry to a one-dimensional model along the x coordinate. The displacement of saponin molecules of molar mass M is given by the Mason-Weaver equation (28), which describes the diffusion and sedimentation under uniform gravity. In our case, sedimentation is completely negligible compared to diffusion because the convective drag force is much smaller than gravity because of the small size of the saponin molecules. Therefore, the Mason-Weaver equation reduces to the classic diffusion equation

$$\frac{\partial C(x,t)}{\partial t} = D\frac{\partial^2 C(x,t)}{\partial x^2}, \tag{3}$$

where $C(x, t)$ is the saponin number concentration at position x and time t and D the diffusion constant of saponins in PBS. For a semi-infinite volume above the uniform cell surface and the apical membrane plane at $x = 0$, the solution of Eq. 3 for an initial concentration C_0 at time $t = 0$ is

$$C(x,t)\ =\ C_0\ \mathrm{erf}\left(\frac{x}{2\sqrt{Dt}}\right), \tag{4}$$

with erf(x) the error function. For a cell surface A, the total number of molecules impinging the surface is then

$$N_0(t)\ =\ A\int_0^\infty [C_0 - C(x,t)]\mathrm{d}x\ =\ \frac{2A\ C_0\sqrt{Dt}}{\sqrt{\pi}}\ =\ \alpha\sqrt{t}. \tag{5}$$

After creation, each pore with initial surface S_{p0} can exponentially increase in size as $S_p(t) = S_{p0}\ e^{t/\tau}$ or exponentially decay as $S_p(t) = S_{p0}\ e^{-t/\tau}$, with τ the characteristic time. At this point, we consider that there is no overlapping of the created pores, so the number of pores is equal to $\eta N_0(t)$, where η is the efficiency, independent of time, of the saponin molecules to create a hole. We introduce the rate of creation of pores

$$j(t) = \eta \frac{dN_0(t)}{dt}. \quad (6)$$

The total surface of pores $\Sigma_p(t)$ for $t > 0$ is given by the convolution between the rate of creation of pores $j(t)$ and the individual surface pore $S_p(t)$ as

$$\Sigma_p(t) = \int_0^t j(u) S_p(t-u) \mathrm{d}u. \quad (7)$$

The created pores allow effusion of molecules from the cytosol according to Fick's first law (29). The number N_c of exiting molecules from the cytosol is then

$$\frac{\mathrm{d}N_c(t)}{\mathrm{d}t} = -\frac{\Sigma_p(t)\, D_c}{V\delta} N_c(t), \quad (8)$$

being the effusion rate for a cell volume V, with D_c the diffusion constant of molecules in the cytosol and δ the plasma membrane thickness. We also define L as the cell thickness so that $V = AL$. After some calculations using Eqs. 5, 7, and 8, one obtains an analytical solution for the normalized evolution of the number of molecules leaking the cytosol for increasing or decaying pore sizes, N_{Inc} and N_{Dec}, respectively:

$$\frac{N_{\mathrm{Inc}}(t)}{N_{c0}} = \exp\left\{-\phi\, \tau^{3/2}\left[\frac{\sqrt{\pi}}{2}\exp\left(\frac{t}{\tau}\right)\mathrm{erf}\sqrt{\frac{t}{\tau}} - \sqrt{\frac{t}{\tau}}\right]\right\}, \quad (9)$$

$$\frac{N_{\mathrm{Dec}}(t)}{N_{c0}} = \exp\left\{-\phi\, \tau^{3/2}\left[\frac{\sqrt{\pi}}{2}\exp\left(\frac{t}{\tau}\right)\mathrm{erfi}\sqrt{\frac{t}{\tau}} - \sqrt{\frac{t}{\tau}}\right]\right\}, \quad (10)$$

with

$$\phi = \frac{2\eta\, C_0 S_{p0} D_c \sqrt{D}}{\sqrt{\pi} L \delta} \quad (11)$$

and with $\mathrm{erf}(x)$ the error function, $\mathrm{erfi} = -i\,\mathrm{erf}(ix)$ the imaginary error function, and N_{c0} the initial number of molecules in the cytosol. Therefore, the population evolution of the lost cytosol molecules depends on two parameters: the exponential pore size evolution time τ and a term ϕ depending on the diffusion constants D_c and D, on the initial saponin concentration C_0, on the cell geometry parameters L and δ, and on the pore parameters S_{p0} and η. However, only a limited number of unknown parameters remain: η, S_{p0}, and τ. The rest of the parameters can be obtained from the literature.

We can notice that the limits of $N_{\mathrm{Inc}}(t)$ and $N_{\mathrm{Dec}}(t)$ for static pores ($1/\tau \to 0$) are both equal to

$$N_{c0}\exp\left[-\frac{2}{3}\phi\, t^{3/2}\right]. \quad (12)$$

We now consider the possible overlapping of the pores during their creation from detergent molecules. Without overlapping, the total surface would continuously increase toward infinity (see Eq. 5), which is not physically relevant. In reality, the total surface of the pores is limited by the available membrane surface. We will analytically treat the limit case of static pores ($1/\tau \to 0$). Let us assume that a surface $\Sigma_p(t)$ of pores was created at the surface membrane. The increase of surface $d\Sigma_p(t)$ is given by the surface ratio probability $S_{p0}\left[1 - \frac{\Sigma_p(t)}{A}\right]$, so one obtains the differential equation for the pore surface evolution considering pore overlapping

$$\frac{d\Sigma_p(t)}{dt} = j(t)\, S_{p0}\left[1 - \frac{\Sigma_p(t)}{A}\right]. \quad (13)$$

Using Eq. 5, the solution of the previous differential equation is, for $t > 0$,

$$\Sigma_p(t) = \eta A\left[1 - \exp\left(-\frac{S_{P0}}{A}\alpha\sqrt{t}\right)\right]. \quad (14)$$

Furthermore, the leakage of cytosol molecules is again calculated using Eq. 8, and we obtain the evolution of the number $N(t)$ of molecules leaking from the cytosol, considering overlapping, for static pores

$$\frac{N(t)}{N_{c0}} = \exp\left\{-\frac{\phi}{f\alpha}\left[t - \frac{1 - e^{-f\alpha\sqrt{t}}\left(1 + f\alpha\sqrt{t}\right)}{\frac{1}{2}f^{\,2}\alpha^2}\right]\right\}, \quad (15)$$

with $f = S_{p0}A$. Here, two mechanisms are opposing. The first is the overlapping of the pores, which results in a decrease of the total pore surface created by the detergent molecules as well as the saturation of the surface to long delays. Its characteristic time is given by Eq. 14 as $t_1 = [A/(S_{p0}\,\alpha)]^2$. The second mechanism is the leakage of the cytosol molecules through the pores because of diffusion and pore size evolution. Equation 12 provides the characteristic time $t_2 = (2\varphi/3)^{-2/3}$. We then define a dimensionless number

$$G = \left(\frac{t_2}{t_1}\right)^{3/2} = \frac{6 S_{p0}^2 C_0^2 D L \delta}{\pi D_c}. \quad (16)$$

Therefore, if $G >> 1$ ($t_1 << t_2$), the limiting factor is the overlapping of the pores, which takes place before the drop of the molecules inside the cell. The effusion rate is then approximately constant. On the contrary, if $G << 1$ ($t_1 >> t_2$), the limiting factor is the diffusion of the cytosol molecules. Hence, the overlapping plays no role. We can notice that $G \propto (D/D_c)$, which is expected because D_c is related to the diffusion of the effusing molecules, whereas D is related to the detergent molecules digging the pores. For instance, if the diffusion of the cytosol molecules is much smaller than that of the detergent molecules, the leakage of the cytosol molecules would remain in the initial linear regime when the overlapping effects begin to be significant.

Finally, using the dimensionless number G, Eq. 15 can be rewritten in a more compact form as

$$\frac{N(t)}{N_{c0}} = e^{3/G}\exp\left[-\frac{Dc\, t}{L\delta} - \frac{3}{G}\left(1 + \sqrt{\frac{t}{\tau_G}}\right)e^{-\sqrt{\frac{t}{\tau_G}}}\right] \quad \text{with} \quad \tau_G = \frac{\pi}{4 S_{p0}^2 C_0^2 D}. \quad (17)$$

RESULTS AND DISCUSSION

We experimented with the effect of the initial concentration of saponins on the membrane permeability dynamics probed by THz-ATR. Before each experiment, the cell support was washed with PBS. For each measurement targeting a given concentration of saponins, a fresh solution of saponin 100

times more concentrated was prepared. The support was put on the THz-ATR prism and allowed to reach room temperature during 15 min at 21°C in 3 mL of PBS. Because the support diameter was 36 mm, the cells were covered by a 3 mm height of solution. Experiments refer to time T after a perturbation was applied to the cells at $T = 0$. We recorded the THz-ATR signal Δ for 30 min to make sure the signal was stable. Then, at $T = 0$, we added 30 μL of 100×-concentrated solution of saponins in PBS with a micropipette so that the resulting saponin concentration equaled c_0. The liquid was pumped in and out several times to homogenize the solution. Then, the THz signal was further recorded during 120–150 min. Typical result versus T is given in Fig. 3. Using least-square regression, the experimental data were fitted with both Eqs. 9 and 10, considering the cases of either pore size increase or decay. The best result from these two equations (see the *red curve* in Fig. 3) provided the parameters τ and φ. In the particular case of parameter τ, we attributed by convention a positive sign if the best fit was obtained from Eq. 9 (size increase) or a negative sign if obtained from Eq. 10 (size decay).

We recorded the THz-ATR dynamics of MDCK cells permeabilization after addition of saponins versus mass concentration c_0 from 10 to 225 μg/mL, so below critical micelle concentration for saponins in water (30). The results are presented in Fig. 4 *A* for parameter φ and Fig. 4 *B* for parameter $1/\tau$. First, for the cell geometry and diffusion parameter φ, a linear dependency versus c_0 is experimentally observed, as expected from Eqs. 1 and 11. Precision at lower concentrations ($c_0 = 5$ μg/mL) was weaker because the amplitude of variation of THz-ATR signal was lower. The slope obtained from Fig. 4 *A* is related to Eqs. 1 and 11 as

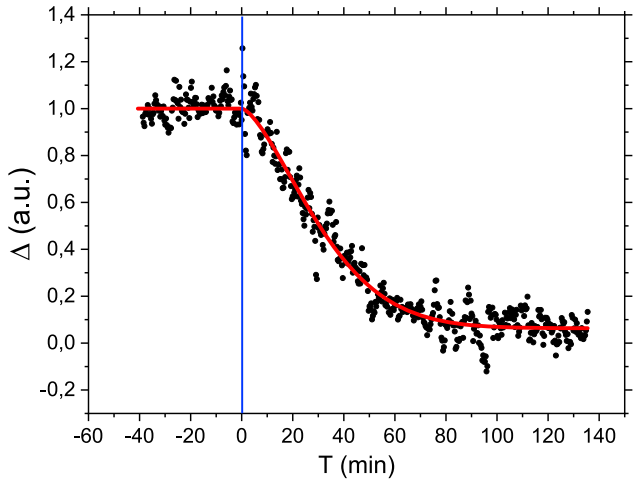

FIGURE 3 THz-ATR signal $\Delta(t)$ for MDCK cell layer after addition of saponins at $T = 0$ for experimental data (*black dots*) and best fit (*red line*). The blue vertical line shows addition of saponin. To see this figure in color, go online.

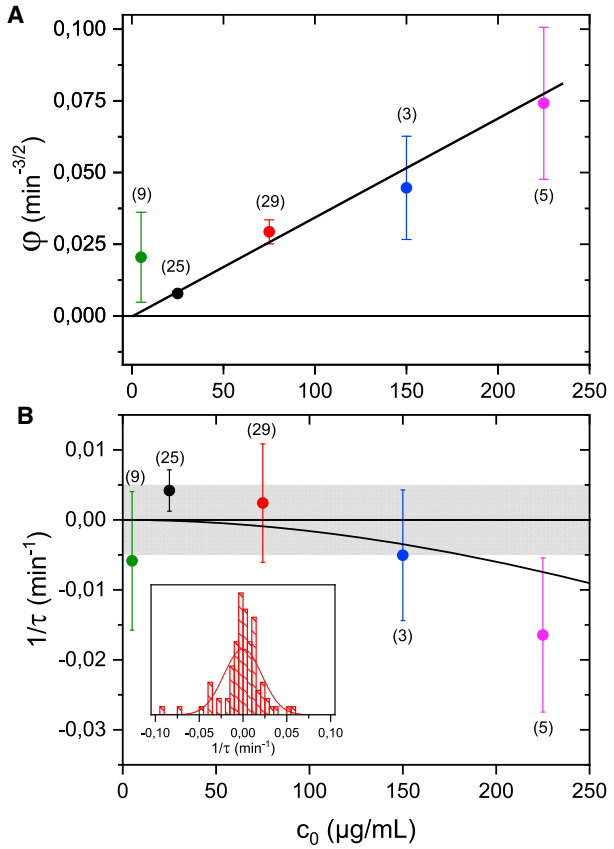

FIGURE 4 Model parameters ϕ (*A*) and $1/\tau$ (*B*) vs. saponin mass concentration c_0. (*A*) The line is the best-fit proportional function. (*B*) The gray rectangle is a guide for the eye. The black line is the apparent $1/\tau$ evolution considering overlapping of the pores. Inset shows the distribution of $1/\tau$ for the whole concentrations and a Gaussian fit. For both, the number of experiments is shown in parentheses. To see this figure in color, go online.

$$\frac{\phi}{c_0} = \frac{2\mathcal{N}_A f\, D_c\sqrt{D}}{\sqrt{\pi}ML\delta}\eta S_{p0}. \tag{18}$$

One finds experimentally that $\phi/c_0 \approx 7.1 \times 10^{-7}$ m^3 g^{-1} s$^{-1.5}$. Using Eq. 18 and the values found in Appendix A, one obtains $\eta S_{p0} \approx 2.3 \times 10^{-5}$ nm^2 (with $f = 0.12$).

In conjunction with an estimate of the size of the micelle-like pore structure formed by saponin in the bonding with cholesterol molecules (22), one can estimate the diameter of the pores to ~4 nm (31), and thus, the pore surface to $S_{p0} = 12.5$ nm^2. Assuming a transverse extension of saponin molecule of 0.6 nm (22), ~20 saponin molecules are found in average in the ring. Then, efficiency $\eta \approx 1.8 \times 10^{-6}$ to form the 20-molecule ring. Also, assuming an individual probability p for a saponin molecule to bind to the membrane, one finds $p^{20} \approx 1.8 \times 10^{-6}$ and then $p \approx 52 \pm 2\%$, considering the uncertainty on the commercial concentration of saponin molecules. This shows that the binding probability to the membrane is very high for the saponin molecules.

TABLE 1 List of Parameter Values

Parameter	Symbol	Value	Unit	Reference
Cell height	L	10	μm	*
Membrane thickness	δ	4	nm	(33)
Cytosol diffusion	D_c	1	$\mu m^2/s$	(34)
Viscosity (water, 300 K)	μ	10^{-3}	Pa.s	(35)
Protein density	ρ	1.37	N/A	(36)
Saponin molar mass	M	1200	g/mol	**
Saponin fraction	f	8–25%	N/A	**

*Confocal microscopy measurements. **Sigma-Aldrich: 47036. N/A, not applicable.

Second, we studied the variation of the pore size evolution characteristic time (see Fig. 4 *B*). At first sight, $1/\tau$ is very close to 0 within experimental uncertainty, shown in gray in Fig. 4 *B*. This corresponds to $|1/\tau| < 0.05$ min^{-1} and then to $|\tau| >$ 200 min. Therefore, pores created by saponins exhibit very slow dynamics, if any, longer than 200 min in any case. Furthermore, Fig. 4 *B* shows an apparent small discrepancy with respect to purely static pores for larger saponin concentration. The experimental values of $1/\tau$ are slightly negative for high saponins concentrations, which would suggest a large, but not infinite, decaying pore size time. However, this appears to be an artifact due to pore overlapping, as shown by the black line, which is the apparent $1/\tau$ evolution considering pore overlapping. This line is obtained by fitting the evolution of the number of leaking cytosol molecules with overlapping and $1/\tau \to 0$ (Eq. 17) by the number of molecules without overlapping (Eq. 10). Because of partial overlapping, the total pore surface becomes slightly smaller than expected, leading to an apparent decay of the pore size. Using the data in Appendix A, one obtains the dimensionless number $G = 1.9 \times 10^{-6} << 1$. This confirms that the limiting factor in our experiments is not the overlapping of pores, but essentially the effusion process. The overall result is then fully compatible with the picture that pores remain static after they are created by saponin molecules, probably because of stable complexes or aggregates of saponin molecules with the membrane cholesterol.

Finally, we can draw a parallel with classical Langmuir-Blodgett trough experiments (30) recording in time the surface pressure of lipid membrane after addition of saponins. The mechanical properties of these lipid films exhibit dynamics quite similar to the one we observed in Fig. 3 and slower when adding cholesterol to the film (0.3 molar fraction). Here, we observe dynamics about twice as slow at similar saponin concentrations, which could be explained by a higher cholesterol concentration (0.5–0.6 molar fraction in epithelial cells (32)). Thus, THz-ATR sensing experiments demonstrate their potential to extend these results to the membrane of living cells.

CONCLUSION

Using terahertz ATR measurements, we followed the leakage of cytosol molecules after permeabilization by saponins. We elaborated a theoretical model involving saponin molecules diffusion, cell geometry, cytosol molecule diffusion, and pore dynamics, which analytically provides evolution equations for the cytosol molecule efflux that depend only on two parameters, one relying on the diffusion and cell geometry parameters and the second on the characteristic evolution time of the created pores. Taking into account overlapping, we also found that two effects are opposing during permeabilization: the pore overlapping related to saponin molecule diffusion and the efflux dynamics of cytosol molecules. The balance between these two mechanisms can be described introducing a dimensionless number. We found a good correlation between the experimental data and the model. In particular, we found that the pores created by saponin molecules appear to be static within experimental uncertainty, and that the probability for a saponin molecule to bind to the membrane is found to be very efficient, with a probability greater than 50%. Therefore, the most limiting parameter in the MDCK permeabilization by saponin molecules is the diffusion of saponin molecules.

APPENDIX A

We present here the relevant parameters (see Table 1) for the model. Furthermore, the diffusion constant D of saponin molecules in the extracellular domain is given by the Stokes-Einstein equation

$$D = \frac{k_B T}{6\pi\mu r_s}, \tag{19}$$

where the Stokes radius r_s is related to the molar mass M of the saponin molecules by

$$r_s = \left[\frac{3M}{4\pi\rho\mathcal{N}_A}\right]^{1/3}, \tag{20}$$

where $\mathcal{N}_A$ is Avogadro's constant. One obtains $D \approx 330$ $\mu m^2/s$.

AUTHOR CONTRIBUTIONS

X.Z. carried out all experiments. G.G. designed the research, carried out the modelization, and wrote the article.

REFERENCES

1. Stewart, M. P., A. Sharei, …, K. F. Jensen. 2016. In vitro and ex vivo strategies for intracellular delivery. *Nature.* 538:183–192.
2. Hapala, I. 1997. Breaking the barrier: methods for reversible permeabilization of cellular membranes. *Crit. Rev. Biotechnol.* 17:105–122.
3. Eeman, M., and M. Deleu. 2010. From biological membranes to biomimetic model membranes. *Biotechnol. Agron. Soc. Environ.* 14:719–736.
4. Ros, U., and A. J. García-Sáez. 2015. More than a pore: the interplay of pore-forming proteins and lipid membranes. *J. Membr. Biol.* 248:545–561.
5. Cooper, S. T., and P. L. McNeil. 2015. Membrane Repair: mechanisms and pathophysiology. *Physiol. Rev.* 95:1205–1240.

6. Poellmann, M. J., and R. C. Lee. 2017. Repair and regeneration of the wounded cell membrane. *Regen. Eng. Transl. Med.* 3:111–132.
7. Rosetti, C. M., G. G. Montich, and C. Pastorino. 2017. Molecular insight into the line tension of bilayer membranes containing hybrid polyunsaturated lipids. *J. Phys. Chem. B.* 121:1587–1600.
8. Breton, M., and L. M. Mir. 2018. Investigation of the chemical mechanisms involved in the electropulsation of membranes at the molecular level. *Bioelectrochemistry.* 119:76–83.
9. Teissie, J., M. Golzio, and M. P. Rols. 2005. Mechanisms of cell membrane electropermeabilization: a minireview of our present (lack of?) knowledge. *Biochim. Biophys. Acta.* 1724:270–280.
10. Ryham, R., I. Berezovik, and F. S. Cohen. 2011. Aqueous viscosity is the primary source of friction in lipidic pore dynamics. *Biophys. J.* 101:2929–2938.
11. Debrégeas, G., P. Martin, and F. Brochard-Wyart. 1995. Viscous bursting of suspended films. *Phys. Rev. Lett.* 75:3886–3889.
12. Islam, M. Z., S. Sharmin, …, M. Yamazaki. 2018. Elementary processes for the entry of cell-penetrating peptides into lipid bilayer vesicles and bacterial cells. *Appl. Microbiol. Biotechnol.* 102:3879–3892.
13. Masson, J. B., M. P. Sauviat, …, G. Gallot. 2006. Ionic contrast terahertz near-field imaging of axonal water fluxes. *Proc. Natl. Acad. Sci. USA.* 103:4808–4812.
14. Shiraga, K., Y. Ogawa, …, M. Imamura. 2014. Characterization of dielectric Responses of human cancer cells in the terahertz region. *J. Infrared Millim. Terahertz Waves.* 35:493–502.
15. Yu, C., S. Fan, …, E. Pickwell-Macpherson. 2012. The potential of terahertz imaging for cancer diagnosis: a review of investigations to date. *Quant. Imaging Med. Surg.* 2:33–45.
16. Woodward, R. M., B. E. Cole, …, M. Pepper. 2002. Terahertz pulse imaging in reflection geometry of human skin cancer and skin tissue. *Phys. Med. Biol.* 47:3853–3863.
17. Masson, J.-B., M.-P. Sauviat, and G. Gallot. 2006. Ionic contrast terahertz time resolved imaging of frog auricular heart muscle electrical activity. *Appl. Phys. Lett.* 89:153904.
18. Grognot, M., and G. Gallot. 2015. Quantitative measurement of permeabilization of living cells by terahertz attenuated total reflection. *Appl. Phys. Lett.* 107:103702.
19. Grognot, M., and G. Gallot. 2017. Relative Contributions of core protein and solvation shell in the terahertz dielectric properties of protein solutions. *J. Phys. Chem. B.* 121:9508–9512.
20. Lang, F., and M. Paulmichl. 1995. Properties and regulation of ion channels in MDCK cells. *Kidney Int.* 48:1200–1205.
21. Puliafito, A., L. Hufnagel, …, B. I. Shraiman. 2012. Collective and single cell behavior in epithelial contact inhibition. *Proc. Natl. Acad. Sci. USA.* 109:739–744.
22. Francis, G., Z. Kerem, …, K. Becker. 2002. The biological action of saponins in animal systems: a review. *Br. J. Nutr.* 88:587–605.
23. Fleck, J. D., A. H. Betti, …, S. G. Verza. 2019. Saponins from *Quillaja saponaria* and *Quillaja brasiliensis*: particular chemical characteristics and biological activities. *Molecules.* 24:24.
24. Wassler, M., I. Jonasson, …, E. Fries. 1987. Differential permeabilization of membranes by saponin treatment of isolated rat hepatocytes. Release of secretory proteins. *Biochem. J.* 247:407–415.
25. Grischkowsky, D., S. R. Keiding, …, C. Fattinger. 1990. Far-infrared time-domain spectroscopy with terahertz beams of dielectrics and semiconductors. *J. Opt. Soc. Am. B.* 7:2006–2015.
26. Podzorov, A., and G. Gallot. 2008. Low-loss polymers for terahertz applications. *Appl. Opt.* 47:3254–3257.
27. Wojdyla, A., and G. Gallot. 2013. Attenuated internal reflection terahertz imaging. *Opt. Lett.* 38:112–114.
28. Mason, M., and W. Weaver. 1924. The settling of small particles in a fluid. *Phys. Rev.* 23:412–426.
29. Crank, J. 1975. The Mathematics of Diffusion, Second Edition. Clarendon Press, Oxford, UK.
30. Korchowiec, B., M. Gorczyca, …, E. Rogalska. 2015. Impact of two different saponins on the organization of model lipid membranes. *Biochim. Biophys. Acta.* 1848:1963–1973.
31. Seeman, P., D. Cheng, and G. H. Iles. 1973. Structure of membrane holes in osmotic and saponin hemolysis. *J. Cell Biol.* 56:519–527.
32. Litvinov, D. Y., E. V. Savushkin, and A. D. Dergunov. 2018. Intracellular and plasma membrane events in cholesterol transport and homeostasis. *J. Lipids.* 2018:3965054.
33. Mitra, K., I. Ubarretxena-Belandia, …, D. M. Engelman. 2004. Modulation of the bilayer thickness of exocytic pathway membranes by membrane proteins rather than cholesterol. *Proc. Natl. Acad. Sci. USA.* 101:4083–4088.
34. Kumar, M., M. S. Mommer, and V. Sourjik. 2010. Mobility of cytoplasmic, membrane, and DNA-binding proteins in *Escherichia coli*. *Biophys. J.* 98:552–559.
35. CRC. 2004. CRC Handbook of Chemistry and Physics 84th Edition, D. R. Lide. CRC Press, Boca Raton, FL.
36. Hinz, H.-J. 1986. Thermodynamic Data for Biochemistry and Biotechnology. Springer-Verlag, Berlin, Heidelberg, Germany.